Applied Catalysis B: Environmental 333 (2023) 122756

Contents lists available at ScienceDirect

Applied Catalysis B: Environmental

journal homepage: www.elsevier.com/locate/apcatb

Temperature hysteresis in dry reforming of methane on Ni/SBA-15 catalyst: Low temperature activity originated from the synergy of Ni^0 and carbon nanotubes

Shenghong Wang [a], Ye Wang [d], Lu Yao [c,*], Changwei Hu [a,b,**]

[a] College of Chemical Engineering, Sichuan University, Chengdu 610065, PR China
[b] Key Laboratory of Green Chemistry and Technology, MOE, College of Chemistry, Sichuan University, Chengdu 610065, PR China
[c] College of Carbon Neutrality Future Technology, Sichuan University, Chengdu 610065, PR China
[d] School of Energy and Power Engineering, Beihang University, Beijing 100191, PR China

ARTICLE INFO

Keywords:
Temperature hysteresis
DRM
Ni/SBA-15
Carbon nanotubes
Low temperature

ABSTRACT

The origins of temperature hysteresis and low temperature activity on Ni/SBA-15 for dry reforming of methane (DRM) were studied. The catalyst structural evolution under different conditions was characterized by Quasi-in-situ XPS, XRD, TG-MS, TEM, and DRM activity test. When heating up in DRM atmosphere, only at 425 °C (ignition temperature, T_{ign}), H_2 and CO were observed, whereas in cooling, the activity dropped to 0% at 295 °C (extinguishing temperature, T_{ext}), forming temperature hysteresis. Below T_{ign}, surface Ni^0 was oxidized to NiO by CO_2 in feed or support oxygen, whereas at T_{ign}, NiO reduction and methane decomposition occurred, generating carbon nanotubes, which improved the oxidation resistance of Ni^0, and the synergetic effect of Ni^0 and carbon nanotubes led to stable activity at about 300 °C. The insight provides basic information for new catalyst design for low temperature activation of both CH_4 and CO_2, and understanding of related phenomena.

1. Introduction

To tackle the expanding threat of global warming affected by greenhouse gas (eg. CH_4 and CO_2), the removal and utilization of CH_4 and CO_2 have been given a lot of attention [1–3]. Dry reforming of methane (DRM) can utilize these two greenhouse gases to produce syngas (H_2 and CO), and the resultant syngas can further be used as a versatile platform for producing high-value chemicals through the Fischer-Tropsch process [4–6]. Therefore, the insight into the catalyst and phenomena of catalysis process for DRM is crucial.

The phenomenon of temperature hysteresis referred to the fact that the ignition temperature (T_{ign}) of the catalystic reaction was different from the extinguishing temperature (T_{ext}) [7–10]. Although hysteresis curves showed similar trends, the mechanism was complex and needed to be studied in detail with targeted experiments.

The hysteresis phenomenon has been explained from the perspectives of the delay phenomenon and the bistability [8,11,12]. Literally, the temperature delay phenomenon was typically derived from the temperature difference during the cooling and heating procedure, which usually occurred in some exothermic reactions, such as CO oxidation and methane oxidation reaction (as listed in Table 1), and originated from the local overheating of the catalyst [10,11,13]. It was reported by Alexander et al. that comparing the catalytic CO oxidation over CuO/-mesh and CuO/Al_2O_3/mesh, the hysteresis of CO oxidation with later catalyst was enhanced because the Al_2O_3 between CuO and mesh hindered the heat dissipation, which confirmed that the local overheating was one of the main reasons for temperature hysteresis [14]. To eliminate the influence of the thermal effect, Alexander's group explored the temperature hysteresis on isobutane dehydrogenation, a group of endothermic reactions (ΔH =130 kJ·mol^{-1}), but no temperature hysteresis signal was observed.

Another proposed reason for temperature hysteresis is the variation of the catalysts' structural transitions [18,25,26], which transforms an input temperature into two outputs steady states [27], that is, bistability or multiplicity [12,18]. Fundamentally, the catalyst's structural transitions was typically contributed from the changing surface state of the adsorbed components [16,28] and the sluggish removal of O_{ads} on the upper surface [15,29]. It was reported that the Pt particles on Pt/ZrO_2 at

* Corresponding author.
** Corresponding author at: College of Chemical Engineering, Sichuan University, Chengdu 610065, PR China.
E-mail addresses: yaolu@scu.edu.cn (L. Yao), changweihu@scu.edu.cn (C. Hu).

https://doi.org/10.1016/j.apcatb.2023.122756
Received 12 February 2023; Received in revised form 9 April 2023; Accepted 10 April 2023
Available online 18 April 2023

Table 1
Overview of typical reactions with temperature hysteresis.

Reaction	Reaction equation	ΔH_R^θ / kJ·mol^{-1}	T_{ign}/ °C	T_{ext}/ °C	Ref.
Partial oxidation of methane (CPOM)	$CH_4 + 1/2\ O_2 \rightarrow CO + 2\ H_2$	-36	450	400	[9, 15]
			518	250	[16]
Oxidative coupling of methane (OCM)	$2CH_4 + O_2 \rightarrow C_2H_4 + 2\ H_2O$	-282	480	160	[17]
			450	375	[18]
Complete oxidation of methane (TOM)	$CH_4 + 2\ O_2 \rightarrow CO_2 + 2\ H_2O$	-802	530	225	[9]
			252	-	[19]
Carbon monoxide oxidation	$2CO + O_2 \rightarrow 2CO_2$	-802	170	145	[12, 13, 20]
			180	-	[21]
Methanation of carbon monoxide	$CO + 3\ H_2 \rightarrow CH_4 + H_2O$	-206	175	130	[22]
NO oxidation	$2NO + O_2 \rightarrow 2NO_2$	-113.8	75	100	[10, 23, 24]

high temperatures sintered seriously, inhibiting the conversion of methane and forming a reverse hysteresis curve [9]. The analysis of in situ NAP-XPS and operando spatially-resolved XAS data revealed that the further reduction of highly dispersed Pd-oxo species would cause partial loss of catalytic performance during the repeated light-off tests [25]. Owing to the lower apparent activation energy of CH_4 reacting with O_{ads} on the Pt surface (60 kJ·mol^{-1}), the sluggish removal of O_{ads} on the catalyst surface could be more effectively in promoting CH_4 oxidation at low temperatures [30]. Chen et al. reported that pure CH_4 pretreatment on 5% Pt/Al_2O_3 lowered the T_{ign} on methane combustion reaction [28], but the T_{ign} of the methane combustion reaction, catalyzed by Pt-CeO_2 catalyst, increased along with the oxygen concentration, owing to the high O_2 concentration that covered the active site during ignition [16]. Are there any other reasons for the occurrence of temperature hysteresis, especially for endothermic reaction? Could any advantages be taken in catalysis research from such performances?

In the present work, it was discovered that DRM, a typical endothermic reaction (ΔH=247 kJ·mol^{-1}), which required high temperature to activate C-H bond in CH_4 and C═O in CO_2 [31,32], exhibited the phenomenon of temperature hysteresis. The origin of this temperature hysteresis in DRM over Ni/SBA-15 catalyst, which showed high stability for DRM, was probed via a series of characterizations of the catalyst samples treated under different conditions. The understanding of the phenomenon might be helpful for the design of new catalysts for low temperature activation of both CH_4 and CO_2.

2. Experimental section

2.1. Catalyst preparation

The catalyst was prepared by impregnation method, which was the same as our previous work [33]. $Ni(NO_3)_2{\cdot}6\ H_2O$ was added into the $NH_3{\cdot}H_2O$ aqueous solution (0.1 mol·L^{-1}) with stirring. Then SBA-15 support was introduced into the above solution. After impregnation for 4 h, the solution was dried by a water bath at 80 ℃. The obtained sample was finally calcined at 800 ℃ for 5 h with the heating rate of 2 ℃·min^{-1} to obtain Ni/SBA-15 catalyst.

2.2. The experiment on temperature hysteresis

The temperature hysteresis experiments of DRM were performed on a fixed-bed continuous flow micro-quartz-tube reactor (10 mm in diameter) with the use of 0.25 g catalyst. The catalyst was reduced at 750 °C for 1 h in the diluted H_2 flow (H_2/Ar=1, F=60 ml·min^{-1}) firstly and the temperature was cooled down to 50 °C. Then, a designated atmosphere (CH_4 and/or CO_2 30 ml·min^{-1}) was introduced into the reaction system. The temperature was increased from 50 °C to 500 °C with a heating rate of 10 °C·min^{-1}. After reaching 500 °C, the heating was stopped and the system was cooled down back to 50 °C in the designated atmosphere (CH_4 and/or CO_2 30 ml·min^{-1}).

The outlet gaseous were analyzed by gas chromatographs online with Plot-C2000 capillary column and TCD detector (Supplement Scheme S1). The conversion of CH_4 and CO_2, the yield of CO and H_2 and the selectivity of H_2 and CO were calculated by the following formulas:

$$X_{CH_4} = \frac{n_{CH_4,in} - n_{CH_4,out}}{n_{CH_4,in}} \times 100\%$$

$$X_{CO_2} = \frac{n_{CO_2,in} - n_{CO_2,out}}{n_{CO_2,in}} \times 100\%$$

$$Y_{H_2} = \frac{n_{H_2}}{2n_{CH_4,in} - 2n_{CH_4,out}} \times 100\%$$

$$Y_{CO} = \frac{nCO}{(n_{CH_4,in} + n_{CO_2,in}) - (n_{CH_4,out} + n_{CO_2,out})} \times 100\%$$

Where, X_{CH4} and X_{CO2} were the conversion of CH_4 and CO_2, respectively. Y_{H2} and Y_{CO} were the yield of H_2 and CO, respectively. $n_{CH4,in}$ and $n_{CO2,in}$ represented the number of moles of CH_4 and CO_2 introduced in the system, while $n_{CH4,out}$, $n_{CO2,in}$, $n_{H2,ou}$ and $n_{CO,out}$ represented the number of mole CH_4, CO_2, H_2 and CO flowed out from the system, respectively.

2.3. Characterization

Quasi-in-situ X-ray photoelectron spectroscopy (XPS) experiments were performed on an AXIS Ultra DLD (KRATOS) spectrometer using mono-chromated Al radiation. The C 1 s peak of 284.6 eV was used to calibrate all the XPS data. After pre-treatment, the samples were directly transferred to the glove box and glued to the sample table. The purpose of this operation was to effectively isolate the influence of air. Then the samples were introduced into the XPS vacuum chamber.

X-ray diffraction (XRD) experiments were carried on DX-1000 CSC diffractometer. Cu Kα was used as X-ray source, tube voltage was 40 kV, the current was 25 mA, and scattering angle range was 10–90°. The average grain size was calculated by the Scherrer formula in MDI Jade 6.5 software.

TG-MS experiments of the catalysts with different treatment methods were carried out on a NETZSCH STA 449 F5 analyzer. Carbon deposition on the used catalysts was analyzed by thermos-gravimetric analysis (TGA) under the dry airflow of 60 ml·min^{-1}, where the sample was heated to 900 °C at the speed of 5 °C·min^{-1}.

Transmission electron microscope (TEM) characterization was performed on Tecnai G2 F20 Twin instrument with a resolution of 0.20 nm and an acceleration voltage of 20 kV. The particle size distribution obtained on TEM was calculated by Nano Measurer software.

3. Result and discussions

3.1. Heating up in DRM atmosphere

The prepared catalyst (Ni/SBA-15) was reduced with H_2, and then the heating/cooling activity experiments were carried out. As shown in Fig. 1, a classical hysteresis was observed when plotting the activity with temperature over Ni/SBA-15 catalyst. Considering the yield of H_2, when heating up in DRM atmosphere, below 425 °C, no H_2 was generated (Fig. 1a), only when the temperature rose to 425 °C, the yield of H_2 rose rapidly from 0% to 2.6%, indicating that the catalyst was not ignited until 425 °C (T_{ign}). When the reaction temperature increased to 500 °C, the yield of H_2 reached 13.6%. When cooling down (also in DRM

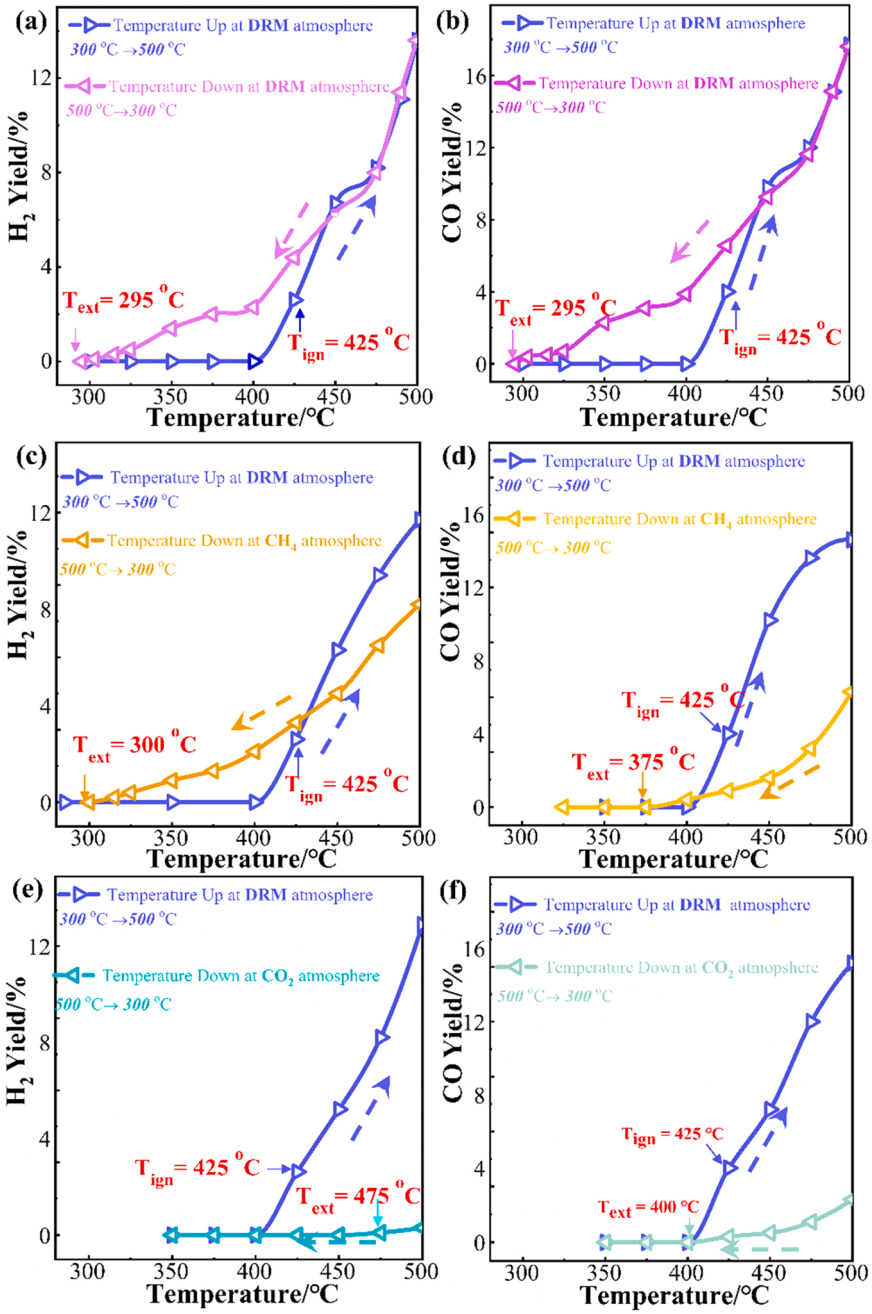

Fig. 1. Hysteresis phenomenon on Ni/SBA-15 catalyst when DRM atmosphere was used as heating atmosphere while DRM atmosphere as cooling down atmosphere: the yield of H_2 (a) and CO (b); while CH_4 as the cooling down atmosphere, the yield of H_2 (c) and CO (d); while CO_2 as the cooling down atmosphere, the yield of H_2 (e), and CO (f).

atmosphere), clearly, the activity almost kept the same with the heating-up process from 500 °C to 450 °C. However, between 450 °C and 300 °C, although the activity gradually decreased with the decrease in reaction temperature, the yields of H_2 were much higher than those obtained at the same temperature when rising, and only when the temperature was around 295 °C, the yield of H_2 approached 0%, which showed 295 °C was T_{ext}. Obviously, the T_{ext} (295 °C) was much lower than T_{ign} (425 °C).

The yield of CO was also suddenly risen from 0% to 4.3% at 425 °C (Fig. 1b), which kept the same variation trend with decreasing temperature as the yield of H_2. The yield dropped to 0% at 290 °C, that is, the T_{ext} of CO was about 290 °C, and the plot of activity with reaction temperature formed an obvious hysteresis.

In order to reconfirm the hysteresis phenomenon, a stability test conducted below T_{ign} was performed on the catalyst (Fig. 2). The catalyst was reduced at 750 °C in H_2 atmosphere, and then cooled to 50 °C in Ar atmosphere, after that, the catalyst was heated in DRM atmosphere, notably, the catalyst was inactive at 400 °C. Whereas, when the reduced catalyst was cooled to 400 °C and 350 °C after heating up to 500 °C in DRM atmosphere, unlike the stage of increasing temperature, the catalyst was still catalytically active at temperatures down to 400 °C and 350 °C, and remained relatively stable during the last 6 h reaction, which was almost the lowest temperature DRM reported so far [34–38].

For further exploring the causes of temperature hysteresis, the single variable experiments were designed. When the mixture of CH_4 and CO_2 was used as the heating atmosphere (DRM atmosphere), the T_{ign} was 425 °C. With the change of cooling down atmosphere, the hysteresis loop and the T_{ext} were different. When CH_4 was the cooling atmosphere,

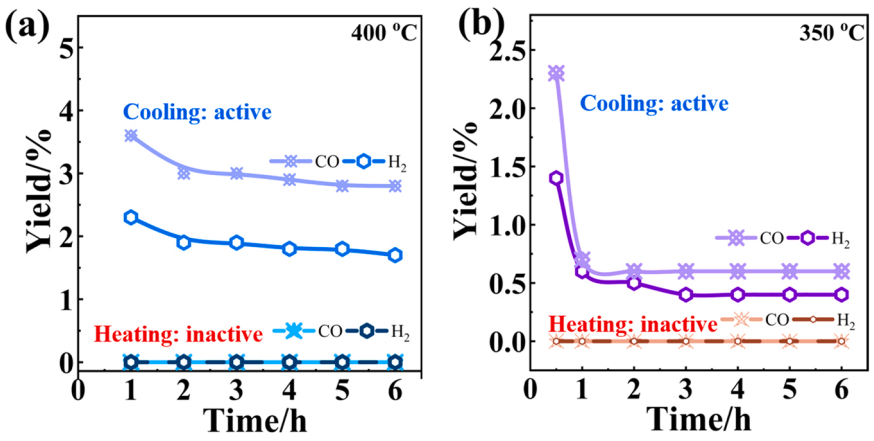

Fig. 2. The catalytic activity of reduced Ni/SBA-15 catalyst in DRM reaction atmosphere: the yield of H_2 and CO when in heating and cooling process at 400 °C (a), and 350 °C (b).

the curve of H_2 yield formed a hysteresis loop, and the T_{ext} was 300 °C (Fig. 1c), whereas the yield of CO was much lower than that of H_2 and turn to 0% at 375 °C (Fig. 1d) because of no O supply. It indicated that the CH_4 atmosphere could be the reason for keeping Ni species of the catalyst active (Ni^0). When CO_2 was the cooling atmosphere, both the curve of the H_2 and CO yield did not exhibit a hysteresis loop (Figs. 1e and 1f). It was indicated that the formation of the hysteresis loop in the cooling process was mainly caused by the existence of CH_4, that is, the CH_4 atmosphere could be the only reason for keeping Ni species of the catalyst active [39–41].

3.2. Heating up in CH_4 atmosphere

When CH_4 was the heating atmosphere, the T_{ign} was also about 425 °C, which showed the same trend of DRM heating atmosphere. Interestingly, there was about 0.5% of CO generated when the temperature increased in the CH_4 atmosphere, which may be caused by the reaction between CH_4 (or the CH_4 decomposition products CH_x) and oxygen in support. When the temperature was cooled down under DRM or CH_4 atmosphere, the hysteresis curve was obtained (Fig. 3a-d). Besides, the yield of CO was 0% until the temperature was cooled down to 310 °C (Fig. 3b) and 350 °C (Fig. 3d), while the H_2 could also be detected when the temperature was below 310 °C (Fig. 3a) and 350 °C (Fig. 3c). When CO_2 was the cooling atmosphere, the CO and H_2 could not be detected at 425 °C (Fig. 3e and f).

3.3. Characterization of the catalysts

In order to explore the changes of surface species, catalysts after reduction, reaction before ignition, reaction at ignition, reaction at 500 °C, reaction before being extinguished, and reaction until being extinguished, were characterized and analyzed, the sign of the samples and the treatments they experienced were indicated in Table 2.

The X-ray diffraction (XRD) results were shown in Fig. 4a. The peaks at 37.2 °, 43.3 °, 62.8 ° and 75.4 ° corresponded to the NiO structure of face-centered cubic [33,42], and the peaks at 44.5 °, 51.8 ° and 76.3 ° were related to the Ni^0 species [43]. Ni^0 was detected on 1# catalyst, indicating that the catalyst was reduced in the reduction stage. Whereas on the 2# catalyst, both NiO and Ni crystal phases existed, which might be attributable to the Ni partly oxidization at low temperature (< 400 °C) by CO_2. When the temperature increased to T_{ign}, there were only typical Ni^0 peaks but without NiO typical peaks on sample 3#. After the reaction was ignited, the samples 3# and 4# kept Ni^0 species constantly without NiO appearing again, even when the temperature was down to a temperature lower than T_{ign} (5#), showing the recovery of Ni^0 in the reaction under these conditions. Furthermore, as the reaction progressed, the peak of C was observed in sample 5#, which might be concerned with the appearance of temperature hysteresis. When the temperature reached T_{ext}, the NiO species appeared again on sample 6#. It is interesting to find that the ignition of the DRM reaction was accompanied by the reduction of NiO, whereas the flameout of the DRM reaction was in step with the appearance of NiO, in other words, the reaction would be maintained with the maintaining of Ni^0. As displayed in Fig. S1, the particle size of 1# ~6# catalysts changes with different processes due to the transformation between Ni and NiO. The above results were also in agreement with the results of catalytic activity (Fig. 1c-d and Fig. 3c-d), which also suggested that the CH_4 atmosphere was the reason for keeping Ni species of the catalyst active (Ni^0).

Quasi-in-situ XPS experiments could provide valuable information for the heterogeneous catalysis [44]. The profiles of the Ni 2p, C 1 s, O 1 s, and Si 2p regions of the XPS spectra were provided in Fig. 4b, c and d. For each sample, there was an asymmetrical Ni 2p3/2 XPS signal that could be deconvoluted into four components at binding energy (BE) values of 851.9, 853.7, 855.2, 856.4, and 860.5 eV (Fig. 4b), which could be assigned to the surface Ni^0, NiO, $Ni(OH)_2$, Ni^{3+} and satellite species, respectively [45–47].

As shown in Fig. 4b, the catalyst after reduction at 750 °C (sample 1#) showed an obvious peak of Ni^0, but no peaks at 853.7 eV (corresponding to NiO species), which was consistent with the XRD results. Whereas, the peak at 852.3 eV disappeared, while the peak at 853.7 eV appeared on sample 2#, indicating that Ni^0 species were oxidized to NiO species in the heating stage in DRM reaction ambiance. The peak of Ni^0 could be observed again when the temperature reached T_{ign} in the reaction atmosphere, where the H_2 yield sharply increased from 0% to 2.6%, showing that NiO reduction and DRM reaction occurred simultaneously on the surface of Ni/SBA-15 catalyst at the ignition point. After ignition, the three peaks corresponding to Ni^0, Ni^{2+} and Ni^{3+} could also be seen on sample 4#, 5#, and 6#, which showed that the metallic Ni^0 and NiO on the surface was mutually transformed during the reaction process.

The XPS spectra of O 1 s at different reaction stages were shown in Fig. 4c. The peak at 533.0 eV corresponded to the binding energy of Si-O bond in SiO_2, which was related to the support. Whereas the peaks at 529.0–531.0 eV corresponded to the binding energy of O^{2-}, that is, the binding energy of O^{2-} in NiO [42]. Where the oxygen in the Ni lattice was easier to migrate and promote the activation of C-H [48]. The binding energy of O^{2-} in samples 1#, 3# and 4# were around 530.7 eV, corresponding to the O combined with Ni on the support. Whereas the binding energy of O^{2-} in samples 2#, 5# and 6# shifted to lower binding energy, with sample 5# shifting by 0.3 eV and samples 2# and 6# shifting by 0.6 eV, mainly related to surface NiO according to XPS spectra of Ni. The binding energy at 103.7 eV of the spectra of Si 2p

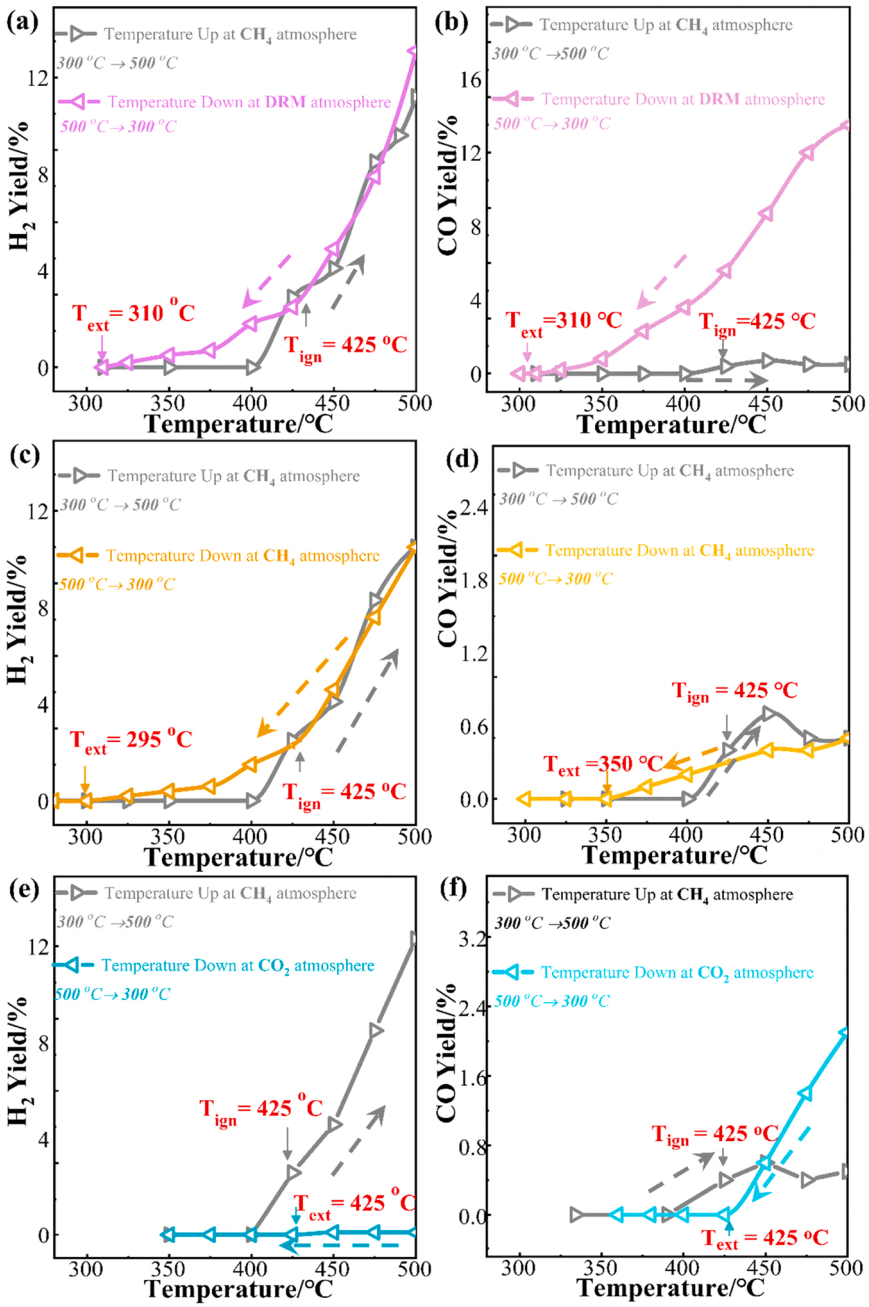

Fig. 3. Hysteresis phenomenon on Ni/SBA-15 catalyst when CH_4 was used as heating atmosphere while cooling down atmosphere was varied. DRM atmosphere was used as cooling down atmosphere: the yield of H_2 (a), the yield of CO (b); CH_4 was used as the cooling down atmosphere, the yield of H_2 (c) and CO (d); CO_2 as the cooling down atmosphere, the yield of H_2 (e), and CO (f).

Table 2
Numbers of samples with different treatment.

Sample	Treatment process	Note
1#	Reducing at 750°C and then cooling to 25 °C in Ar atmosphere	Fresh
2#	1# heating to 400 °C in DRM atmosphere	$<T_{ign}$
3#	1# heating to 425 °C in DRM atmosphere	T_{ign}
4#	1# heating to 500 °C in DRM atmosphere	500 °C
5#	4# cooling down to 425 °C in DRM atmosphere	Cooling
6#	4# cooling down to 295 °C in DRM atmosphere	T_{ext}

corresponded to Si-O in SiO_2 support (Fig. S2) [49], and the valence of Si had not changed during the reaction, which showed that the formation of hysteresis rings had little relationship with the SiO_2 support.

Three kinds of C signal peaks could be obtained in the C 1 s spectra (Fig. 4d). The peaks at 288.2 eV might be originated from the sp^2-hybridized adventitious carbon, e.g., C-O (epoxy carbon or hydroxyl) and C═O (carboxylic carbon), and the peaks at 282.6 eV may be ascribed to the sp^2 C atoms of C-Si-O in graphitic carbon, which might be formed on the SiO_2 support [50,51], and mainly occurred in the early stages of carbon nanotubes (CNTs) formation (Fig. 4d). The peaks at 282.6 eV and 288.2 eV were observed in samples 4#, 5#, and 6#, indicating that after the ignition reaction, CNTs may be generated and combine with Ni in the cooling process. In the stage below the ignition temperature, the formation of CNTs maybe beneficial to the oxidation resistance of Ni^0, making the catalyst active for DRM.

The surface content of Ni and C was calculated and shown in Table 3. For sample 1#, the surface content of Ni^0 was about 1.13%, and the total

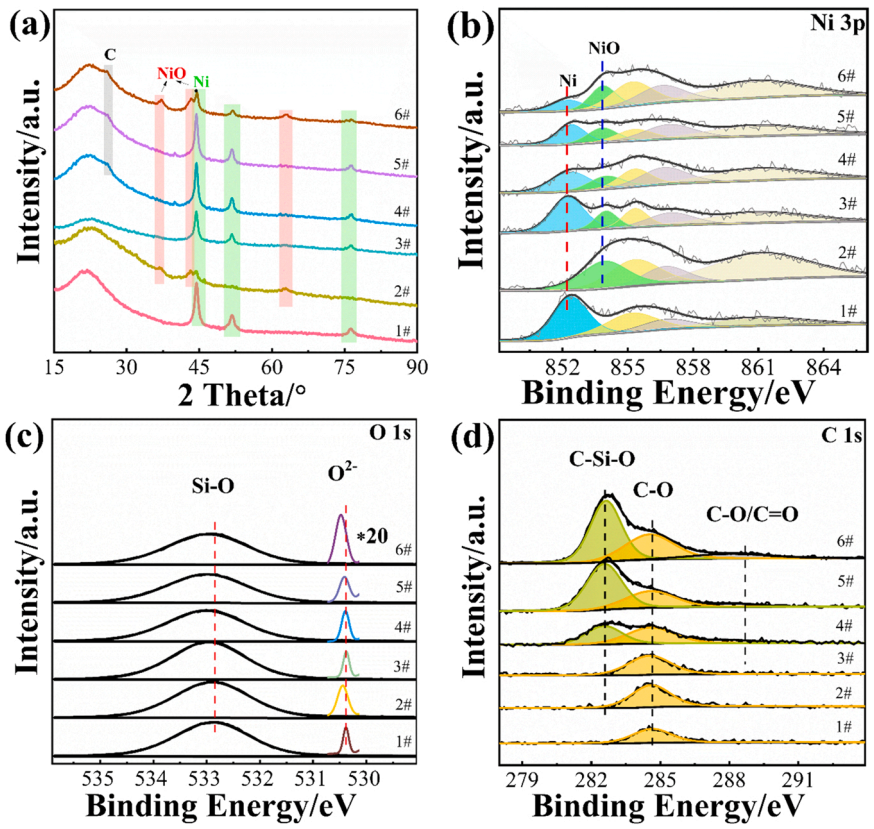

Fig. 4. The XRD pattern (a), the XPS spectra of Ni 2p (b), O 1 s (c), and C 1 s (d) on the Ni /SBA-15 catalysts at the different reaction stages.

Table 3
The content of Ni, O, and C species on the Ni/SBA-15 catalyst with different treatment.

Species	Relative content /%[a]					
	1#	2#	3#	4#	5#	6#
Ni^0	1.13	0.00	1.08	0.79	0.56	0.28
NiO	0.00	1.13	0.40	0.45	0.44	0.52
$Ni(OH)_2$	0.72	1.23	0.43	0.58	0.44	0.83
Total Ni^{2+}	0.72	2.36	0.83	1.03	0.88	1.35
Total Ni	2.25	3.09	2.50	2.65	2.22	2.37
CNT	0.00	0.00	0.00	4.90	8.69	10.66
C-C	4.30	5.86	5.16	5.63	5.70	5.59
C-O	0.00	0.00	0.00	1.18	1.62	1.12

of Ni^{2+} was about 0.72%. Whereas Ni^0 was not detected on the surface of sample 2#, while the content of NiO plus Ni $(OH)_2$ increased from 0.72% to 2.36%. It indicated that when heating 1# to 400 °C in DRM atmosphere, Ni^0 might be transformed to NiO or Ni $(OH)_2$. Notably, the metallic Ni^0 species was detected again on sample 3#, and the surface content of Ni^0 was about 1.08%, whereas the content of $NiO/Ni(OH)_2$ decreased from 1.13% and 1.23–0.4% and 0.43%, respectively. Besides, the surface content of Ni^{2+} gradually increased but the content of Ni^0 gradually decreased in catalyst 4# when the temperature rose to 500 °C. At T_{ext}, the content of Ni^0 reduced to 0.28% on 6#. In addition, the change of O 1 s spectra from sample 1# to 6# could provide clues of the changes between metal states to oxide state. As we all know, Ni^0 was the active metal, which directly affected the proceeding of the reaction. The decreasing content of Ni^0 resulted in the deactivation of the catalyst. It was found that without CNTs, Ni species mainly existed as NiO at the corresponding temperature (2#), while Ni species could maintain the Ni^0 state after CNTs being formed (3#−6#). It would be speculated that the oxidation of Ni was inhibited, or the recovery of Ni^0 was promoted by CNTs, which might cause the temperature hysteresis of DRM reaction, where Ni/SBA-15 catalyst exhibited DRM activity at much lower temperature (about 300 ℃).

TG-MS experiments (in air atmosphere) were carried out for samples of different treatment (Fig. 5a). After reduction, sample 1# showed a tendency to gain weight due to the oxidation of metal Ni^0. In sample 2#, the trend of weight gain was less obvious than that of sample 1#, mainly because part of Ni metal had been oxidized to NiO during the heating process, which was consistent with the above results of XPS and XRD. The weight gain trend was also observed on sample 3#, which was stronger than that on sample 2#, indicating that a portion of NiO on sample 3# was reduced to Ni^0 after heating to 425 °C, but no mass loss nor MS signal were observed indicating no carbon deposition, which might be due to the short reaction time. On samples 4#, 5# and 6#, obvious mass loss was detected, and the weight loss gradually increased from 4# to 6#. In addition, only obvious MS signal of CO_2 was detected in the three samples, indicating that the oxidation of carbon was the main cause of the weight loss. Besides, the peak of CO_2 on samples 4#, 5#, and 6# was mainly at about 550 °C, reconfirming the formation of CNTs [52,53].

TEM and HR-TEM characterization were carried on the sample after the hysteresis test (Fig. 5b). NiO (200) crystal plane was found, but without a lattice spacing about 0.182 nm corresponding to the Ni^0 crystal plane, which further proved that the deactivation of the catalyst at the T_{ext} was the lack of Ni^0. CNTs were observed on the catalyst after hysteresis test, and Ni species were observed at the tip of CNTs, indicating the formation of the unique structure between Ni and CNTs. The CNTs may modify the structure of Ni/SABA-15 catalyst [54].

3.4. Possible reaction process

According to the above discussion, the hysteresis that occurred on the DRM reaction was mainly caused by $Ni^0 \leftrightarrow Ni^{2+}$ cycle, and the formation of CNTs. CNTs and the co-existence of Ni formed a new unique

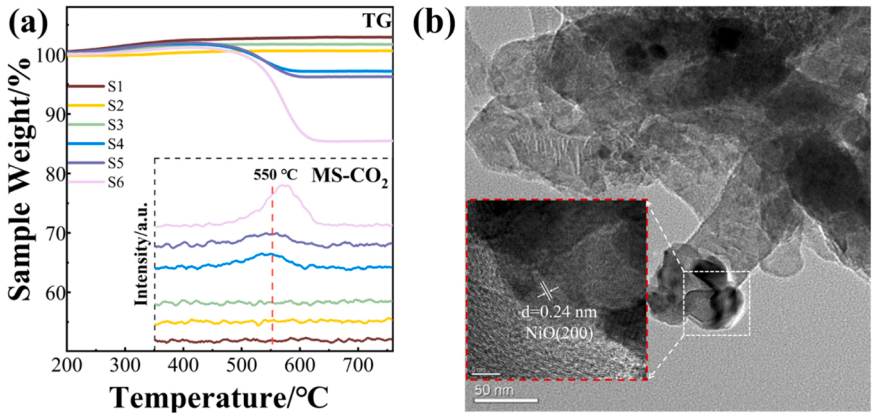

Fig. 5. TG and MS patterns of Ni/SBA-15 catalyst with different treatments (a), and the TEM images after hysteresis reaction (b).

catalyst structure, improving the ability of oxidation resistance of Ni at low temperatures, therefore co-catalyzed DRM at a much lower temperature. Therefore, the possible reaction processes in the temperature hysteresis phenomenon were proposed and shown in Scheme 1.

Before the T_{ign}, since the Ni^0 was oxidized by CO_2 in the presence of CH_4, the DRM reaction could not be ignited because of the lacking of Ni^0, then no H_2 formation was observed. At T_{ign}, in the DRM atmosphere, CH_4 decomposed even on partially oxidized catalyst surface, and surface NiO was in situ reduced to Ni^0 at the same time, with H_2 generation. The formed H_2 could reduce NiO to Ni^0, and then Ni^0 would further catalyze the DRM reaction to produce H_2 and CO, which led to the sharp DRM reaction at 425 °C. Therefore, a dramatic rise in yield of H_2 and CO was observed (Fig. 1). Generally, the formation of CNTs is a disadvantage of Ni-based DRM catalysts, which will expand the catalyst bed, and eventually clog the reactor. However, in the present work, it was found that, the CNTs formation may be positive for DRM at low temperature. After ignition of DRM reaction, CNTs were formed subsequently, and new unique catalyst structure combining CNTs and Ni species was established on the surface gradually. The new catalyst exhibited DRM activity at rather low temperature, that is the reason that even below T_{ign}, the newly formed catalyst could still catalyze the DRM reaction, because Ni^0 could be recycled in the presence of CNTs at low reaction temperature (about 300 °C). However, when the temperature was decreased to 295 °C, the Ni^0 could be oxidized by CO_2 to NiO, which could not be reduced by CH_4 in DRM atmosphere even in the presence of CNTs, then the yield of CO was about 0%, indicating the extinction of DRM reaction. That is, Ni^0 species is capable of activating and converting CH_4 at about 300 °C via DRM if it could be restored, which provides some information for new catalyst design for the activation and conversion of both CH_4 and CO_2 at low temperature.

4. Conclusion

There was a temperature hysteresis phenomenon over Ni/SBA-15 catalyst for DRM reaction. The T_{ign} was 425 °C and T_{ext} was 295 °C, that is, in the process of heating up, only when the temperature reached 425 °C, H_2 and CO were observed. During the cooling process, the activity gradually decreased with decreasing temperature and dropped to 0% until 295 °C. Through tracking the catalyst structure, oxidation state evolutions of Ni species, and linking the hysteresis phenomenon with the reaction atmosphere during DRM reaction, it was concluded that the occurrence of temperature hysteresis was associated with the Ni/SBA-15 catalyst structural transitions. Below T_{ign}, the surface metal Ni^0 was oxidized to NiO, which cannot promote the reaction, and at T_{ign}, NiO reduction and methane decomposition reactions occurred simultaneously. In the catalytic process after the ignition, CNTs were generated, which modified the structure of Ni/SBA-15 catalyst, forming new catalytic species, improving the ability of oxidation resistance or recovery of

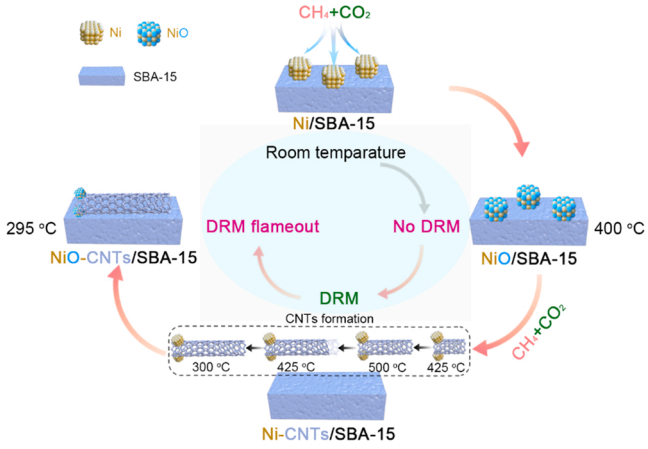

Scheme 1. Schematic diagram of the variation of catalyst in DRM hysteresis reaction under different conditions.

the metal Ni. When the temperature was lower than T_{ext}, the reaction stopped because the CH_4 cannot continue to reduce NiO, and then the balance between NiO and Ni^0 conversion was broken.

CRediT authorship contribution statement

Shenghong Wang: Experiments, Formal analysis, Writing – original draft. **Ye Wang:** Methodology, Data curation. **Lu Yao:** Results analysis, Writing – review & editing. **Changwei Hu:** Supervision, Writing – review & editing, Funding acquisition.

Declaration of Competing Interest

The authors declare that they have no known competing financial interests or personal relationships that could have appeared to influence the work reported in this paper.

Data availability

Data will be made available on request.

Acknowledgements

This work was financially supported by the National Key R&D Program of China (No. 2018YFB1501404), 111 Project (B17030) and Fundamental Research Funds for Central Universities. We thank Yunfei Tian of the analytical & testing center of Sichuan University for XPS experiments and Shanling Wang of the analytical & testing center of

Sichuan University for XRD experiments.

Appendix A. Supporting information

Supplementary data associated with this article can be found in the online version at doi:10.1016/j.apcatb.2023.122756.

References

[1] D. Liang, Y. Wang, M. Chen, X. Xie, C. Li, J. Wang, et al., Dry reforming of methane for syngas production over attapulgite-derived MFI zeolite encapsulated bimetallic Ni-Co catalysts, Appl. Catal. B-Environ. 322 (2023), 122088, https://doi.org/10.1016/j.apcatb.2022.122088.

[2] G. Sneddon, A. Greenaway, H.H. Yiu, The potential applications of nanoporous materials for the adsorption, separation, and catalytic conversion of carbon dioxide, Adv. Energy Mater. 4 (2014), 1301873, https://doi.org/10.1002/aenm.201301873.

[3] Q. Wang, W. Wang, M. Cao, S. Li, P. Wang, J. He, et al., Effect of interstitial carbon atoms in core-shell $Ni_3ZnC_{0.7}/Al_2O_3$ catalyst for high-performance dry reforming of methane, Appl. Catal. B-Environ. 317 (2022), 121806, https://doi.org/10.1016/j.apcatb.2022.121806.

[4] H. Qu, H. Yang, L. Han, S. He, J. Liu, R. Hu, et al., Sandwich-structured nickel/kaolinite catalyst with boosted stability for dry reforming of methane with carbon dioxide, Chem. Eng. J. 453 (2023), 139694, https://doi.org/10.1016/j.cej.2022.139694.

[5] R. Zhou, M. Mohamedali, Y. Ren, Q. Lu, N. Mahinpey, Facile synthesis of multi-layered nanostructured ni/ceo_2 catalyst plus in-situ pre-treatment for efficient dry reforming of methane, Appl. Catal. B-Environ. 316 (2022), 121696, https://doi.org/10.1016/j.apcatb.2022.121696.

[6] Q. Song, R. Ran, X. Wu, Z. Si, D. Weng, Dry reforming of methane over Ni catalysts supported on micro- and mesoporous silica, J. CO_2 Util. 68 (2023), 102387, https://doi.org/10.1016/j.jcou.2022.102387.

[7] D.C. Spray, D.B. Belkin, Heart rate-cloacal temperature hysteresis in iguana is a result of thermal lag, Nature 239 (1972) 337–338, https://doi.org/10.1038/239337a0.

[8] M. Yamaguchi, Thermal hysteresis involving reversible self-catalytic reactions, Acc. Chem. Res. 54 (2021) 2603–2613, https://doi.org/10.1021/acs.accounts.1c00090.

[9] J.D. Grunwaldt, N. van Vegten, A. Baiker, Insight into the structure of supported palladium catalysts during the total oxidation of methane, Chem. Commun. (2007) 4635–4637, https://doi.org/10.1039/b710222d.

[10] W. Hauptmann, M. Votsmeier, J. Gieshoff, A. Drochner, H. Vogel, Inverse hysteresis during the no oxidation on pt under lean conditions, Appl. Catal. B-Environ. 93 (2009) 22–29, https://doi.org/10.1016/j.apcatb.2009.09.008.

[11] F. Bin, X. Wei, B. Li, K.S. Hui, Self-sustained combustion of carbon monoxide promoted by the Cu-Ce/ZSM-5 catalyst in $CO/O_2/N_2$ atmosphere, Appl. Catal. B-Environ. 162 (2015) 282–288, https://doi.org/10.1016/j.apcatb.2014.07.007.

[12] R.M. Al Soubaihi, K.M. Saoud, J. Dutta, Critical review of low-temperature CO oxidation and hysteresis phenomenon on heterogeneous catalysts, Catalysts 8 (2018) 660, https://doi.org/10.3390/catal8120660.

[13] P.A. Carlsson, M. Skoglundh, Low-temperature oxidation of carbon monoxide and methane over alumina and ceria supported platinum catalysts, Appl. Catal. B-Environ. 101 (2011) 669–675, https://doi.org/10.1016/j.apcatb.2010.11.008.

[14] A.N. Subbotin, B.S. Gudkov, V.I. Yakerson, S.V. Chertkova, E.Z. Golosman, G. V. Kozyreva, Temperature-hysteresis effects in CO oxidation on cement catalysts with various CuO content, Russ. J. Appl. Chem. 74 (2001) 1506–1508, https://doi.org/10.1023/A:1013753118042.

[15] D.D. Nogare, S. Salemi, P. Biasi, P. Canu, Taking advantage of hysteresis in methane partial oxidation over Pt on honeycomb monolith, Chem. Eng. Sci. 66 (2011) 6341–6349, https://doi.org/10.1016/j.ces.2011.04.029.

[16] J.H. Jin, C. Li, C.W. Tsang, B. Xu, C.H. Liang, Catalytic combustion of methane over Pt-Ce oxides under scarce oxygen condition, Ind. Eng. Chem. Res. 55 (2016) 2293–2301, https://doi.org/10.1021/acs.iecr.5b04202.

[17] D. Noon, A. Seubsai, S. Senkan, Oxidative coupling of methane by nanofiber catalysts, ChemCatChem 5 (2013) 146–149, https://doi.org/10.1002/cctc.201200408.

[18] A. Aseem, G.G. Jeba, M.T. Conato, J.D. Rimer, M.P. Harold, Oxidative coupling of methane over mixed metal oxide catalysts: steady state multiplicity and catalyst durability, Chem. Eng. J. 331 (2018) 132–143, https://doi.org/10.1016/j.cej.2017.08.093.

[19] Z. Boukha, A. Choya, M. Cortés-Reyes, B. de Rivas, L.J. Alemany, J.R. González-Velasco, et al., Influence of the calcination temperature on the activity of hydroxyapatite-supported palladium catalyst in the methane oxidation reaction, Appl. Catal. B: Environ. 277 (2020), 119280, https://doi.org/10.1016/j.apcatb.2020.119280.

[20] J. Dong, Y. Zhang, D. Li, A. Adogwa, S. Huang, M. Yang, et al., Reaction-driven evolutions of Pt states over Pt-CeO_2 catalysts during CO oxidation, Appl. Catal. B: Environ. 330 (2023), 122662, https://doi.org/10.1016/j.apcatb.2023.122662.

[21] E.A. Lashina, E.M. Slavinskaya, N.A. Chumakova, A.I. Stadnichenko, A.N. Salanov, G.A. Chumakov, et al., Inverse temperature hysteresis and self-sustained oscillations in CO oxidation over Pd at elevated pressures of reaction mixture: experiment and mathematical modeling, Chem. Eng. Sci. 212 (2020), 115312, https://doi.org/10.1016/j.ces.2019.115312.

[22] A.N. Subbotin, I.R. Subbotina, E.Z. Golosman, Hysteresis phenomena in heterogeneous exothermal catalytic reactions and methods for decreasing the overheating of catalyst nanoclusters, Mendeleev Commun. 25 (2015) 216–218, https://doi.org/10.1016/j.mencom.2015.05.020.

[23] A. Arvajová, P. Kočí, V. Schmeißer, M. Weibel, The impact of CO and C_3H_6 pulses on PtOx reduction and NO oxidation in a diesel oxidation catalyst, Appl. Catal. B-Environ. 181 (2016) 644–650, https://doi.org/10.1016/j.apcatb.2015.08.004.

[24] A. Buzková Arvajová, P. Boutikos, R. Pečinka, P. Kočí, Global kinetic model of no oxidation on Pd/γ-Al_2O_3 catalyst including PdOx formation and reduction by CO and C_3H_6, Appl. Catal. B-Environ. 260 (2020), 118141, https://doi.org/10.1016/j.apcatb.2019.118141.

[25] V. Muravev, J.F.M. Simons, A. Parastaev, M.A. Verheijen, J.J.C. Struijs, N. Kosinov, et al., Operando spectroscopy unveils the catalytic role of different palladium oxidation states in CO oxidation on Pd/CeO_2 catalysts, Angew. Chem. Int. Ed. 61 (2022), e202200434, https://doi.org/10.1002/anie.202200434.

[26] B.K. Miller, P.A. Crozier, Linking changes in reaction kinetics and atomic-level surface structures on a supported Ru catalyst for CO oxidation, ACS Catal. 11 (2021) 1456–1463, https://doi.org/10.1021/acscatal.0c03789.

[27] X. Zhang, Y. Deng, P. Tian, H. Shang, J. Xu, Y. Han, Dynamic active sites over binary oxide catalysts: in situ/operando spectroscopic study of low-temperature CO oxidation over MnOx-CeO_2 catalysts, Appl. Catal. B-Environ. 191 (2016) 179–191, https://doi.org/10.1016/j.apcatb.2016.03.030.

[28] L.X. Chen, J.P. McCann, S.L. Tait, A re-examination of the catalyst activation and temperature hysteresis in methane combustion on Pt/Al_2O_3, Appl. Catal. A-Gen. 549 (2018) 19–30, https://doi.org/10.1016/j.apcata.2017.09.008.

[29] W.H. Chen, Y.C. Cheng, C.I. Hung, Enhancement of heat recirculation on the hysteresis effect of catalytic partial oxidation of methane, Int. J. Hydrog. Energy 38 (2013) 10394–10406, https://doi.org/10.1016/j.ijhydene.2013.05.057.

[30] E. Poffe, H. Kaper, B. Ehrhardt, L. Gigli, D. Aubert, L. Nodari, et al., Understanding oxygen release from nanoporous perovskite oxides and its effect on the catalytic oxidation of CH_4 and CO, ACS Appl. Mater. Interfaces 13 (2021) 25483–25492, https://doi.org/10.1021/acsami.1c02281.

[31] A. Kurlov, E.B. Deeva, P.M. Abdala, D. Lebedev, A. Tsoukalou, A. Comas-Vives, et al., Exploiting two-dimensional morphology of molybdenum oxycarbide to enable efficient catalytic dry reforming of methane, Nat. Commun. 11 (2020) 4920, https://doi.org/10.1038/s41467-020-18721-0.

[32] C. Palmer, D.C. Upham, S. Smart, M.J. Gordon, H. Metiu, E.W. McFarland, Dry reforming of methane catalysed by molten metal alloys, Nat. Catal. 3 (2020) 83–89, https://doi.org/10.1038/s41929-019-0416-2.

[33] S. Wang, Y. Wang, C. Hu, The effect of $nh_3{\cdot}h_2o$ addition in Ni/SBA-15 catalyst preparation on its performance for carbon dioxide reforming of methane to produce H_2, Int. J. Hydrog. Energy 43 (2018) 13921–13930, https://doi.org/10.1016/j.ijhydene.2018.01.173.

[34] Z. Liu, P. Lustemberg, R.A. Gutiérrez, J.J. Carey, R.M. Palomino, M. Vorokhta, et al., In situ investigation of methane dry reforming on metal/ceria (111) surfaces: metal-support interactions and C-H bond activation at low temperature, Angew. Chem. Int. Ed. 56 (2017) 13041–13046, https://doi.org/10.1002/anie.201707538.

[35] J. Yang, D. Gong, X. Lu, C. Han, H. Liu, L. Wang, Ni-CeO_2/SBA-15 catalyst prepared by glycine-assisted impregnation method for low-temperature dry reforming of methane, Crystals 12 (2022), https://doi.org/10.3390/cryst12050713.

[36] S. Kim, J. Lauterbach, E. Sasmaz, Yolk-shell Pt-NiCe@SiO_2 single-atom-alloy catalysts for low-temperature dry reforming of methane, ACS Catal. 11 (2021) 8247–8260, https://doi.org/10.1021/acscatal.1c01223.

[37] Z. Song, Q. Wang, C. Guo, S. Li, W. Yan, W. Jiao, et al., Improved effect of fe on the stable NiFe/Al_2O_3 catalyst in low-temperature dry reforming of methane, Ind. Eng. Chem. Res. 59 (2020) 17250–17258, https://doi.org/10.1021/acs.iecr.0c01204.

[38] A.H.K. Owgi, A.A. Jalil, M.A.A. Aziz, W. Nabgan, N.S. Hassan, I. Hussain, et al., The preferable ni quantity to boost the performance of FSA for dry reforming of methane, Fuel 332 (2023), 126124, https://doi.org/10.1016/j.fuel.2022.126124.

[39] A.P. Ramon, X. Li, A.H. Clark, O.V. Safonova, F.C. Marcos, E.M. Assaf, et al., In situ study of low-temperature dry reforming of methane over $La_2Ce_2O_7$ and $LaNiO_3$ mixed oxides, Appl. Catal. B-Environ. 315 (2022), 121528, https://doi.org/10.1016/j.apcatb.2022.121528.

[40] A. Chatla, F. Abu-Rub, A.V. Prakash, G. Ibrahim, N.O. Elbashir, Highly stable and coke-resistant Zn-modified Ni-Mg-Al hydrotalcite derived catalyst for dry reforming of methane: synergistic effect of Ni and Zn, Fuel 308 (2022), 122042, https://doi.org/10.1016/j.fuel.2021.122042.

[41] C. Wang, T. Su, Z. Qin, H. Ji, Coke-resistant Ni-based bimetallic catalysts for the dry reforming of methane: effects of indium on the Ni/Al_2O_3 catalyst, Catal. Sci. Technol. 12 (2022) 4826–4836, https://doi.org/10.1039/D2CY00582D.

[42] Y. Wang, L. Yao, Y.N. Wang, S.H. Wang, Q. Zhao, D.H. Mao, et al., Low-temperature catalytic CO_2 dry reforming of methane on Ni-Si/ZrO_2 catalyst, ACS Catal. 8 (2018) 6495–6506, https://doi.org/10.1021/acscatal.8b00584.

[43] L. Yao, M.E. Galvez, C.W. Hu, P. Da Costa, Mo-promoted Ni/Al_2O_3 catalyst for dry reforming of methane, Int. J. Hydrog. Energy 42 (2017) 23500–23507, https://doi.org/10.1016/j.ijhydene.2017.03.208.

[44] I.V. Yentekakis, G. Goula, M. Hatzisymeon, I. Betsi-Argyropoulou, G. Botzolaki, K. Kousi, et al., Effect of support oxygen storage capacity on the catalytic performance of rh nanoparticles for CO_2 reforming of methane, Appl. Catal. B-Environ. 243 (2019) 490–501, https://doi.org/10.1016/j.apcatb.2018.10.048.

[45] Y. Wang, R. Zhang, B. Yan, Ni/$Ce_{0.9}Eu_{0.1}O_{1.95}$ with enhanced coke resistance for dry reforming of methane, J. Catal. 407 (2022) 77–89, https://doi.org/10.1016/j.jcat.2022.01.020.

[46] Y. Lu, L. Kang, D. Guo, Y. Zhao, Y. Zhao, S. Wang, et al., Double-site doping of a v promoter on Ni_x-V-MgAl catalysts for the drm reaction: simultaneous effect on CH_4

and CO_2 activation, ACS Catal. 11 (2021) 8749–8765, https://doi.org/10.1021/acscatal.1c01299.
[47] K. Jeon, J.K. Kim, B. Kim, W. Jang, Y.C. Kang, H. Roh, Ultra-stable porous yolk-shell Ni catalysts for the steam reforming of methane with alkali poisoning, Chem. Eng. J. 454 (2023), 140060, https://doi.org/10.1016/j.cej.2022.140060.
[48] E. Genty, J. Brunet, C. Poupin, S. Ojala, S. Siffert, R. Cousin, Influence of Co addition on the toluene total oxidation over Co based mixed oxide catalysts, Appl. Catal. B-Environ. 247 (2019) 163–172, https://doi.org/10.1016/j.apcatb.2019.01.081.
[49] M. Li, Z. Sun, Y.H. Hu, Catalysts for CO_2 reforming of CH_4: a review, J. Mater. Chem. A 9 (2021) 12495–12520, https://doi.org/10.1039/D1TA00440A.
[50] S. Wang, Z. Li, G. Wang, Y. Wang, Z. Ling, C. Li, Freestanding $Ti_3C_2T_x$ mxene/prussian blue analogues films with superior ion uptake for efficient capacitive deionization by a dual pseudocapacitance effect, ACS Nano 16 (2022) 1239–1249, https://doi.org/10.1021/acsnano.1c09036.
[51] X. Liu, Z. Xu, C. Chen, D. Tian, L. Yang, X. Luo, et al., Carbon quantum dot-sensitized and tunable luminescence of $Ca_{19}Mg_2(PO_4)_{14}$:In^{3+} (In^{3+}= Eu^{3+} and/or Tb^{3+}) nanocrystalline phosphors with abundant colors via a sol-gel process, J. Mater. Chem. C. 7 (2019) 2361–2375, https://doi.org/10.1039/C8TC06599C.
[52] C. Jin, T.C. Nagaiah, W. Xia, B. Spliethoff, S. Wang, M. Bron, et al., Metal-free and electrocatalytically active nitrogen-doped carbon nanotubes synthesized by coating with polyaniline, Nanoscale 2 (2010) 981–987, https://doi.org/10.1039/B9NR00405J.
[53] L.M. Esteves, A.A. Daás, H.A. Oliveira, F.B. Passos, Influence of space velocity and catalyst pretreatment on co_x free hydrogen and carbon nanotubes production over CoMo/MgO catalyst, Int. J. Hydrog. Energy 45 (2020) 27299–27311, https://doi.org/10.1016/j.ijhydene.2020.07.133.
[54] O. Kwon, A.C. Foucher, R. Huang, E.A. Stach, J.M. Vohs, R.J. Gorte, Evidence for redispersion of Ni on $LaMnO_3$ films following high-temperature oxidation, J. Catal. 407 (2022) 213–220, https://doi.org/10.1016/j.jcat.2022.01.036.